

# A Finite Difference Frequency Domain Based Full Vectorial Transverse Modesolver for Anisotropic Waveguides with Arbitrary Permittivity and Permeability Tensors

Varun Singh

Department of Electrical Engineering  
Indian Institute of Technology Madras, Chennai, Tamil Nadu, 600036, India  
varunsingh316@gmail.com, ee11d025@ee.iitm.ac.in

**Abstract** — In this work a Yee's mesh based full vectorial transverse finite difference frequency (FDFD) modesolver has been derived from discretized Maxwell's equations in Matrix form for anisotropic waveguides with arbitrary permittivity and permeability tensors. This work incorporates arbitrary permittivity and permeability simultaneously into matrix equations of Yee's mesh based modesolver, which previous works have not done. For benchmarking the Python implementation of these matrix equations, cross section of Yitrium Iron Garnate (YIG) channel waveguide has been taken as first one of the three test structures. Numerical result from this work has been compared with that from previous work on YIG channel waveguide and is found to be in good agreement. Further, for benchmarking the effective index values of waveguides having both permittivity and permeability anisotropic simultaneously, a finite element based commercial software (COMSOL) has been used, the values of effective indexes from solver presented in this work and commercial software have been compared, and are also found to be in good agreement.

**Index Terms** — Anisotropic waveguides, finite difference frequency domain, full vectorial, modesolver.

## I. INTRODUCTION

Despite finite difference time domain (FDTD) method being the most general purpose and robust method for simulation of Nanophotonic and Integrated Optic devices, finite difference frequency domain (FDFD) method is also very useful in solving some Nanophotonic and Integrated Optic problems such as single mode verification, coupling length calculations etc. Moreover the mode field solutions obtained from a Yee's mesh based FDFD modesolver are more compatible with Yee's mesh based propagation methods for the purpose of mode launching. The previous works on transverse FDFD modesolvers [1-5] have not incorporated arbitrary permittivity and permeability tensors simultaneously into their formulation but this work incorporates arbitrary

permittivity and permeability tensors simultaneously into formulation of FDFD based transverse modesolver.

In order to benchmark accuracy of the solver, numerically calculated effective index from the solver presented here has been compared with effective index given in [4] for Yttrium Iron Garnate (YIG) channel waveguide. Moreover effective indexes of waveguides having both permeability and permeability anisotropic simultaneously have also been calculated and compared with values given by finite element based commercial software [6].

## II. THEORY AND MATRIX FORMULATIONS

While deriving the matrix equations for modesolver the convention for naming variables is same as in [5]. The Maxwell's equations are written assuming  $e^{i(\beta z - \omega t)}$  dependence (where  $\beta = 2\pi \frac{N_{eff}}{\lambda}$  and  $k_0 = 2\pi/\lambda$ , with  $\lambda$  being free space wavelength) which leads to  $\frac{\partial}{\partial z} = i\beta$  and  $\frac{\partial}{\partial t} = -i\omega$ .  $N_{eff}$  contains both real and imaginary part of scaled eigen solution (scaled by  $\lambda/2\pi$ ). The real part of this solution is denoted by  $n_{eff}$  (effective index), also electric fields are scaled by the impedance of free space. Further all permittivity and permeability values used here are relative.

The Maxwell's equations with above conditions applied are:

$$ik_0 \varepsilon_{xx} H_x + ik_0 \varepsilon_{xy} H_y + ik_0 \varepsilon_{xz} H_z = \frac{\partial E_z}{\partial y} - i\beta E_y, \quad (1)$$

$$ik_0 \mu_{yx} H_x + ik_0 \mu_{yy} H_y + ik_0 \mu_{yz} H_z = i\beta E_x - \frac{\partial E_z}{\partial x}, \quad (2)$$

$$ik_0 \mu_{zx} H_x + ik_0 \mu_{zy} H_y + ik_0 \mu_{zz} H_z = \frac{\partial E_y}{\partial x} - \frac{\partial E_x}{\partial y}, \quad (3)$$

$$-ik_0 \varepsilon_{xx} E_x - ik_0 \varepsilon_{xy} E_y - ik_0 \varepsilon_{xz} E_z = \frac{\partial H_z}{\partial y} - i\beta H_y, \quad (4)$$

$$-ik_0 \varepsilon_{yx} E_x - ik_0 \varepsilon_{yy} E_y - ik_0 \varepsilon_{yz} E_z = i\beta H_x - \frac{\partial H_z}{\partial x}, \quad (5)$$

$$-ik_0 \varepsilon_{zx} E_x - ik_0 \varepsilon_{zy} E_y - ik_0 \varepsilon_{zz} E_z = \frac{\partial H_y}{\partial x} - \frac{\partial H_x}{\partial y}, \quad (6)$$

Now discretizing the fields in above equations in accordance with Yee's meshing scheme, the fields can

be represented as,  $E_x \rightarrow E_x(j+1/2, 1)$ ,  $E_y \rightarrow E_y(j, 1+1/2)$ ,  $E_z \rightarrow E_z(j, 1)$ ,  $H_x \rightarrow H_x(j, 1+1/2)$ ,  $H_y \rightarrow H_y(j+1/2, 1)$ ,  $H_z \rightarrow H_z(j+1/2, 1+1/2)$ . Now writing the discretized Maxwell's equations into matrix form (with bold symbols representing matrix variables) leads to:

$$ik_0 \begin{bmatrix} \boldsymbol{\mu}_{xx} & \boldsymbol{\mu}_{xy} & \boldsymbol{\mu}_{xz} \\ \boldsymbol{\mu}_{yx} & \boldsymbol{\mu}_{yy} & \boldsymbol{\mu}_{yz} \\ \boldsymbol{\mu}_{zx} & \boldsymbol{\mu}_{zy} & \boldsymbol{\mu}_{zz} \end{bmatrix} \begin{bmatrix} \mathbf{H}_x \\ \mathbf{H}_y \\ \mathbf{H}_z \end{bmatrix} = \begin{bmatrix} \mathbf{0} & -i\beta\mathbf{I} & \mathbf{U}_y \\ i\beta\mathbf{I} & \mathbf{0} & -\mathbf{U}_x \\ -\mathbf{U}_y & \mathbf{U}_x & \mathbf{0} \end{bmatrix} \begin{bmatrix} \mathbf{E}_x \\ \mathbf{E}_y \\ \mathbf{E}_z \end{bmatrix}, \quad (7)$$

$$-ik_0 \begin{bmatrix} \boldsymbol{\varepsilon}_{xx} & \boldsymbol{\varepsilon}_{xy} & \boldsymbol{\varepsilon}_{xz} \\ \boldsymbol{\varepsilon}_{yx} & \boldsymbol{\varepsilon}_{yy} & \boldsymbol{\varepsilon}_{yz} \\ \boldsymbol{\varepsilon}_{zx} & \boldsymbol{\varepsilon}_{zy} & \boldsymbol{\varepsilon}_{zz} \end{bmatrix} \begin{bmatrix} \mathbf{E}_x \\ \mathbf{E}_y \\ \mathbf{E}_z \end{bmatrix} = \begin{bmatrix} \mathbf{0} & -i\beta\mathbf{I} & \mathbf{V}_y \\ i\beta\mathbf{I} & \mathbf{0} & -\mathbf{V}_x \\ -\mathbf{V}_y & \mathbf{V}_x & \mathbf{0} \end{bmatrix} \begin{bmatrix} \mathbf{H}_x \\ \mathbf{H}_y \\ \mathbf{H}_z \end{bmatrix}, \quad (8)$$

In the above matrix Eqs. (7) and (8),  $\boldsymbol{\varepsilon}_{xx}$ ,  $\boldsymbol{\varepsilon}_{yy}$ , ... and  $\boldsymbol{\mu}_{xx}$ ,  $\boldsymbol{\mu}_{yy}$ , ... are all diagonal square matrices with diagonal size equal to the number of field computation points in the simulation window.  $\mathbf{U}_x$ ,  $\mathbf{U}_y$ ,  $\mathbf{V}_x$  and  $\mathbf{V}_y$  are Yee's mesh based differential operators in sparse square matrix form, the size of these matrices is equal to square of the number of field computation points in the simulation window. For this work  $\mathbf{U}_x$  and  $\mathbf{U}_y$  are given by Eqs. (9) and (10) respectively,  $\mathbf{V}_x$  and  $\mathbf{V}_y$  can be derived from  $\mathbf{U}_x$  and  $\mathbf{U}_y$  respectively, by transferring the smaller diagonal to lower triangular region while keeping the offset from the main diagonal unchanged, followed by change of sign in both diagonals. Here the offset in  $\mathbf{U}_x$  is one and in  $\mathbf{U}_y$ , it is equal to number of field computation points along  $x$  direction. The above matrices have also been described in [6]:

$$\mathbf{U}_x = \frac{1}{\Delta x} \begin{bmatrix} -1 & 1 & & \\ & -1 & \ddots & \\ & & \ddots & \ddots \\ & & & \ddots & \ddots \end{bmatrix}, \quad (9)$$

$$\mathbf{U}_y = \frac{1}{\Delta y} \begin{bmatrix} -1 & & & & \\ & 1 & & & \\ & & -1 & & \\ & & & \ddots & \\ & & & & \ddots & \ddots \end{bmatrix}, \quad (10)$$

$\mathbf{E}_x$ ,  $\mathbf{E}_y$ ,  $\mathbf{E}_z$  and  $\mathbf{H}_x$ ,  $\mathbf{H}_y$ ,  $\mathbf{H}_z$  are field matrices which contain the mode field values and their size is equal to the number of field computation points in the simulation window. It is worth mentioning here that the number of field computation points will be dictated by discretizations  $\Delta x$  and  $\Delta y$  in  $x$  and  $y$  directions respectively. Further the field matrices have been stored in row-major order. After careful algebraic manipulations (substitutions &

eliminations) on matrix Eqs. (7) and (8), they get reduced to Eigen equation given by Eq. (11). It is worth mentioning here that Eqs:

$$\beta \begin{bmatrix} \mathbf{E}_x \\ \mathbf{E}_y \\ \mathbf{H}_x \\ \mathbf{H}_y \end{bmatrix} = \begin{bmatrix} \mathbf{F}_{11} & \mathbf{F}_{12} & \mathbf{F}_{13} & \mathbf{F}_{14} \\ \mathbf{F}_{21} & \mathbf{F}_{22} & \mathbf{F}_{23} & \mathbf{F}_{24} \\ \mathbf{F}_{31} & \mathbf{F}_{32} & \mathbf{F}_{33} & \mathbf{F}_{34} \\ \mathbf{F}_{41} & \mathbf{F}_{42} & \mathbf{F}_{43} & \mathbf{F}_{44} \end{bmatrix} \begin{bmatrix} \mathbf{E}_x \\ \mathbf{E}_y \\ \mathbf{H}_x \\ \mathbf{H}_y \end{bmatrix}, \quad (11)$$

where

$$\mathbf{F}_{11} = i\boldsymbol{\mu}_{yz}(\boldsymbol{\mu}_{zz})^{-1}\mathbf{U}_y + i\mathbf{U}_x(\boldsymbol{\varepsilon}_{zz})^{-1}\boldsymbol{\varepsilon}_{zx}, \quad (12)$$

$$\mathbf{F}_{12} = -i\boldsymbol{\mu}_{yz}(\boldsymbol{\mu}_{zz})^{-1}\mathbf{U}_x + i\mathbf{U}_x(\boldsymbol{\varepsilon}_{zz})^{-1}\boldsymbol{\varepsilon}_{zy}, \quad (13)$$

$$\mathbf{F}_{13} = k_0\boldsymbol{\mu}_{yx} - k_0\boldsymbol{\mu}_{yz}(\boldsymbol{\mu}_{zz})^{-1}\boldsymbol{\mu}_{zx} - (k_0)^{-1}\mathbf{U}_x(\boldsymbol{\varepsilon}_{zz})^{-1}\mathbf{V}_y, \quad (14)$$

$$\mathbf{F}_{14} = k_0\boldsymbol{\mu}_{yy} - k_0\boldsymbol{\mu}_{yz}(\boldsymbol{\mu}_{zz})^{-1}\boldsymbol{\mu}_{zy} + (k_0)^{-1}\mathbf{U}_x(\boldsymbol{\varepsilon}_{zz})^{-1}\mathbf{V}_x, \quad (15)$$

$$\mathbf{F}_{21} = -i\boldsymbol{\mu}_{xz}(\boldsymbol{\mu}_{zz})^{-1}\mathbf{U}_y + i\mathbf{U}_y(\boldsymbol{\varepsilon}_{zz})^{-1}\boldsymbol{\varepsilon}_{zx}, \quad (16)$$

$$\mathbf{F}_{22} = i\boldsymbol{\mu}_{xz}(\boldsymbol{\mu}_{zz})^{-1}\mathbf{U}_x + i\mathbf{U}_y(\boldsymbol{\varepsilon}_{zz})^{-1}\boldsymbol{\varepsilon}_{zy}, \quad (17)$$

$$\mathbf{F}_{23} = -k_0\boldsymbol{\mu}_{xx} + k_0\boldsymbol{\mu}_{xz}(\boldsymbol{\mu}_{zz})^{-1}\boldsymbol{\mu}_{zx} - (k_0)^{-1}\mathbf{U}_y(\boldsymbol{\varepsilon}_{zz})^{-1}\mathbf{V}_y, \quad (18)$$

$$\mathbf{F}_{24} = -k_0\boldsymbol{\mu}_{xy} + k_0\boldsymbol{\mu}_{xz}(\boldsymbol{\mu}_{zz})^{-1}\boldsymbol{\mu}_{zy} + (k_0)^{-1}\mathbf{U}_y(\boldsymbol{\varepsilon}_{zz})^{-1}\mathbf{V}_x, \quad (19)$$

$$\mathbf{F}_{31} = -k_0\boldsymbol{\varepsilon}_{yx} + k_0\boldsymbol{\varepsilon}_{yz}(\boldsymbol{\varepsilon}_{zz})^{-1}\boldsymbol{\varepsilon}_{zx} + (k_0)^{-1}\mathbf{V}_x(\boldsymbol{\mu}_{zz})^{-1}\mathbf{U}_y, \quad (20)$$

$$\mathbf{F}_{32} = -k_0\boldsymbol{\varepsilon}_{yy} + k_0\boldsymbol{\varepsilon}_{yz}(\boldsymbol{\varepsilon}_{zz})^{-1}\boldsymbol{\varepsilon}_{zy} - (k_0)^{-1}\mathbf{V}_x(\boldsymbol{\mu}_{zz})^{-1}\mathbf{U}_x, \quad (21)$$

$$\mathbf{F}_{33} = i\boldsymbol{\varepsilon}_{yz}(\boldsymbol{\varepsilon}_{zz})^{-1}\mathbf{V}_y + i\mathbf{V}_x(\boldsymbol{\mu}_{zz})^{-1}\boldsymbol{\mu}_{zx}, \quad (22)$$

$$\mathbf{F}_{34} = -i\boldsymbol{\varepsilon}_{yz}(\boldsymbol{\varepsilon}_{zz})^{-1}\mathbf{V}_x + i\mathbf{V}_x(\boldsymbol{\mu}_{zz})^{-1}\boldsymbol{\mu}_{zy}, \quad (23)$$

$$\mathbf{F}_{41} = k_0\boldsymbol{\varepsilon}_{xx} - k_0\boldsymbol{\varepsilon}_{xz}(\boldsymbol{\varepsilon}_{zz})^{-1}\boldsymbol{\varepsilon}_{zx} + (k_0)^{-1}\mathbf{V}_y(\boldsymbol{\mu}_{zz})^{-1}\mathbf{U}_y, \quad (24)$$

$$\mathbf{F}_{42} = k_0\boldsymbol{\varepsilon}_{xy} - k_0\boldsymbol{\varepsilon}_{xz}(\boldsymbol{\varepsilon}_{zz})^{-1}\boldsymbol{\varepsilon}_{zy} - (k_0)^{-1}\mathbf{V}_y(\boldsymbol{\mu}_{zz})^{-1}\mathbf{U}_x, \quad (25)$$

$$\mathbf{F}_{43} = -i\boldsymbol{\varepsilon}_{xz}(\boldsymbol{\varepsilon}_{zz})^{-1}\mathbf{V}_y + i\mathbf{V}_y(\boldsymbol{\mu}_{zz})^{-1}\boldsymbol{\mu}_{zx}, \quad (26)$$

$$\mathbf{F}_{44} = i\boldsymbol{\varepsilon}_{xz}(\boldsymbol{\varepsilon}_{zz})^{-1}\mathbf{V}_x + i\mathbf{V}_y(\boldsymbol{\mu}_{zz})^{-1}\boldsymbol{\mu}_{zy}, \quad (27)$$

(12)-(27) are much more generalized equations than previously published works[1-3, 5], as previous works on transverse FDFD Yee's mesh based modesolvers can only handle arbitrarily anisotropic permittivity but not arbitrarily anisotropic permeability. Moreover this solver is also capable of handling anisotropic permittivity and permeability simultaneously which previous Yee's mesh based modesolvers have not addressed. The boundary conditions currently used assume zero field values outside the simulation window. It is worth pointing out here that future works based on this work will explore incorporation of modern boundary conditions such as surface impedance absorbing boundary conditions (SIABC) [7] and subgridding [8] for reducing the memory requirements for this solver.

Further it is also worth pointing out here that all programs for this work have been written in Python by making use of Python-scipy's (Version - 0.13.3) sparse linear algebra eigen value and eigen vector finder (which uses ARPACK library) with shift invert mode enabled. The wavelength ( $\lambda$ ) used in channel waveguide simulations

is  $1.3 \mu\text{m}$ , while the wavelength used in the other two test cases is  $1.55 \mu\text{m}$ .

### III. RESULTS AND COMPARISONS

For comparisons and benchmarking the first test structure [4], which has been used here is cross section of a YIG (Yttrium Iron Garnate) channel waveguide placed in air/vacuum with anisotropic rectangular core as shown in Fig. 1.

The anisotropic rectangular core of channel waveguide has height of  $607.6 \text{ nm}$  and is  $800 \text{ nm}$  wide. It has isotropic permeability but its relative permittivity tensor has five terms which are  $-\epsilon_{xx}=\epsilon_{yy}=\epsilon_{zz} = 2.302^2$ ,  $\epsilon_{xy} = i\Delta$  and  $\epsilon_{yx} = -i\Delta$ . The magnitude ( $\Delta$ ) of non-diagonal terms is  $0.005$ . The substrate has isotropic refractive index of  $1.95(n_1)$  for this waveguide. For effective index calculation a simulation window of  $3.2 \mu\text{m} \times 2.9 \mu\text{m}$  with discretization of  $7.5 \text{ nm}$  in both  $x$  and  $y$  directions has been used as opposed to  $6.25 \text{ nm} \times 4.9 \text{ nm}$  discretization in [4] due to memory constraints but future works based on this work will handle this problem by utilizing advanced subgridding algorithms such as mentioned in [8]. The effective index of fundamental mode as given in [4] for the YIG channel waveguide is  $2.0488$ . The effective index of the same fundamental mode as calculated by Yee's mesh based solver described in this work is  $2.0483$ .

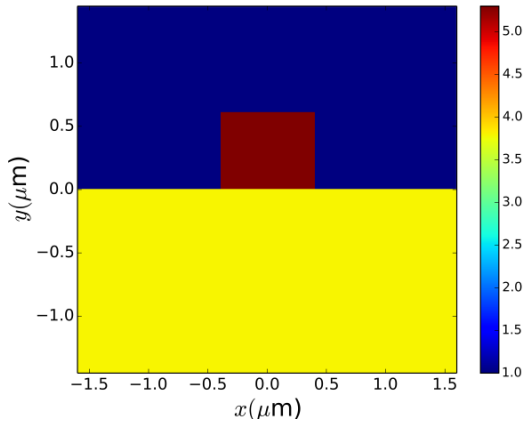


Fig. 1. Permittivity profile and structure of channel waveguide with anisotropic core (the central rectangular area).

The second test structure which has been used here for benchmarking is a rectangular waveguide with anisotropic core having a height of  $180 \text{ nm}$  and width of  $300 \text{ nm}$ . This waveguide is surrounded by an isotropic medium with relative permittivity equal to  $2.0736(1.44^2)$  as shown in Fig. 2. This waveguide has both permittivity and permeability anisotropic simultaneously with  $\mu_{xx} = \mu_{yy} = \mu_{zz} = 1.0$ ,  $\mu_{xy} = i0.2$ ,  $\mu_{yx} = -i0.2$  and  $\epsilon_{xx} = \epsilon_{yy} = \epsilon_{zz} = 12.1104(3.48^2)$ ,  $\epsilon_{xy} = i0.2$ ,  $\epsilon_{yx} = -i0.2$ ,

rest of the terms in relative permittivity and relative permeability are zero.

The simulation window used in simulation of anisotropic rectangular waveguide of Fig. 2 with Yee's mesh based modesolver implemented for this work is  $3 \mu\text{m} \times 3 \mu\text{m}$  with a discretization of  $15 \text{ nm}$  in both  $x$  and  $y$  directions. For benchmarking, commercial finite element based software [6] has been used, element size in the software has been set at  $15 \text{ nm}$  and the simulation window size has been kept at  $3 \mu\text{m} \times 3 \mu\text{m}$ . The effective index value of the fundamental mode as given by commercial software [6] is  $1.7377$  while its value given by solver implemented for this work in Python is  $1.7415$ .

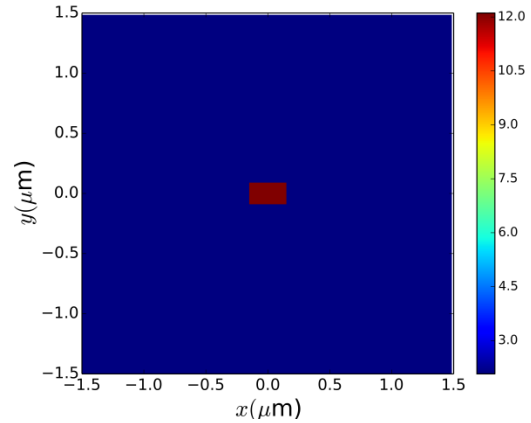


Fig. 2. Permittivity profile and structure of rectangular waveguide with anisotropic core (the central area).

The third test structure which has been used here for benchmarking is a square waveguide with anisotropic core having a height of  $300 \text{ nm}$  and width of  $300 \text{ nm}$ . This waveguide is also surrounded by an isotropic medium with relative permittivity equal to  $2.0736(1.44^2)$  as shown in Fig. 3. This waveguide also has both permittivity and permeability anisotropic simultaneously with  $\mu_{xx} = 1.5625(1.25^2)$ ,  $\mu_{yy} = 1.44(1.2^2)$ ,  $\mu_{zz} = 1.21(1.1^2)$ ,  $\mu_{xy} = i0.3$ ,  $\mu_{yx} = -i0.3$ ,  $\mu_{xz} = 0.15$ ,  $\mu_{zx} = 0.15$ ,  $\mu_{zy} = -i0.25$ ,  $\mu_{yz} = i0.25$  and  $\epsilon_{xx} = 12.1104(3.48^2)$ ,  $\epsilon_{yy} = 10.24(3.2^2)$ ,  $\epsilon_{zz} = 9.0(3.0^2)$ ,  $\epsilon_{xy} = i0.2$ ,  $\epsilon_{yx} = -i0.2$ ,  $\epsilon_{xz} = 0.1$ ,  $\epsilon_{zx} = 0.1$ ,  $\epsilon_{yz} = i0.1$ ,  $\epsilon_{zy} = -i0.1$ .

The simulation window used for Yee's mesh based simulation of the third structure with this solver as well as commercial software[6] is same as in the simulation of second test structure ( $3 \mu\text{m} \times 3 \mu\text{m}$ ). The  $x$  and  $y$  discretizations for this solver as well as element size in commercial software [6] has been kept at  $15 \text{ nm}$ . The effective index value of the fundamental mode as given by commercial software [6] is  $2.7980$ , while its value as given by solver implemented for this work is  $2.8124$ . Its worth pointing out here that the values of terms in permittivity and permeability matrices in second and

third test cases above were chosen randomly for the purpose of comparison and benchmarking the waveguides with both permittivity and permeability anisotropic simultaneously. Table 1 sums up the benchmarking for this work.

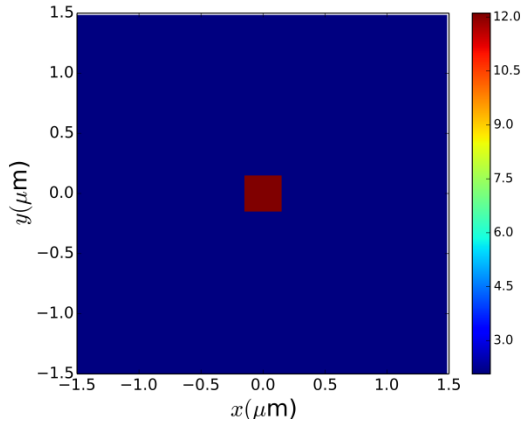


Fig. 3. Permittivity profile and structure of square waveguide with anisotropic core (the central area).

Table 1: Comparison of effective indexes of anisotropic waveguides taken from this work and other sources

Structure	$n_{eff}$ (Other Sources)	$n_{eff}$ (This Work)
Channel waveguide	2.0488 [4]	2.0483
Rectangular waveguide	1.7377 [6]	1.7415
Square waveguide	2.7980 [6]	2.8124

#### IV. CONCLUSION

In this work a transverse FDFD modesolver which can handle arbitrary permittivity as well as permeability simultaneously has been implemented in Python. Further waveguides with anisotropic core with both permittivity and permeability anisotropic simultaneously have also been analyzed which the previous works [1-5] on FDFD modesolver have not done. The capability to handle arbitrarily anisotropic permeability and permittivity simultaneously is unique and novel feature of this work. Future works based on this work will mainly focus on incorporating modern as well as advanced boundary conditions [7] and subgridding [8] algorithms in the

solver. Further combining this solver with modal expansion methods will also be explored in the future.

#### ACKNOWLEDGMENT

The author would like to thank Ministry of Human Resource Development (MHRD), Government of India, for funding this work.

#### REFERENCES

- [1] Z. Zhu and T. G. Brown, "Full-vectorial finite difference analysis of microstructured optical fibers," *Optics Express*, vol. 10, no. 17, pp. 853-864, August 2002.
- [2] C.-P. Yu and H.-C. Chang, "Yee's-mesh-based finite difference eigenmode solver with PML absorbing boundary conditions for optical waveguides and photonic crystal fibers," *Optics Express*, vol. 12, no. 25, pp. 6165-6177, December 2004.
- [3] M.-Y. Chen, S.-M. Hsu, and H.-C. Chang, "A finite-difference frequency domain method for full vectorial mode solutions of anisotropic optical waveguides with an arbitrary permittivity tensor," *Optics Express*, vol. 17, no. 8, pp. 5965-5979, April 2009.
- [4] A. B. Fallahkhair, K. S. Li, and T. E. Murphy, "Vector finite-difference modesolver for anisotropic dielectric waveguides," *Journal of Light-wave Technology*, vol. 26, no. 11, pp. 1423-1431, June 2008.
- [5] V. Singh, "A Yee's mesh based modesolver for anisotropic waveguides," *2016 IEEE/ACES International Conference on Wireless Information Technology and Systems (ICWITS) and Applied Computational Electromagnetics (ACES)*, pp. 1-2, March 2016.
- [6] <https://www.comsol.co.in/wave-optics-module>
- [7] Y. Mao, A. Z. Elsherbeni, S. Li, and T. Jiang, "Surface impedance absorbing boundary terminating FDTD simulations," *Applied Computational Electromagnetics Society Journal*, vol. 29, no. 12, pp. 1035-1046, December 2014.
- [8] G. Kim, E. Arvas, V. Demir, and A. Z. Elsherbeni, "A novel nonuniform subgridding scheme for FDTD using an optimal interpolation technique," *Progress in Electromagnetics Research*, vol. 44, pp. 137-161, September 2012.